JOURNAL OF APPLIED POLYMER SCIENCE VOL. 20, 1005–1023 (1976)

Extrudate Swell During the Melt Spinning of Fibers—Influence of Rheological Properties and Take-up Force

JAMES L. WHITE and JOSEPH F. ROMAN,* *Department of Chemical and Metallurgical Engineering, The University of Tennessee, Knoxville, Tennessee 37916*

Synopsis

A theoretical and experimental study has been carried out on extrudate swell B, especially the influence of rheological properties and applied take-up force on the emerging melt. The problem is analyzed in terms of (1) dimensional analysis, (2) force–momentum balances, (3) partially constrained elastic recovery. Analyses in terms of force–momentum balances are only able to give extrudate swell B in the asymptote of high Reynolds numbers. For low Reynolds numbers, they simply relate the take-up force to the pressure field in the spinneret. Increasing the take-up force predicts a decrease in the exit pressure. The partially constrained elastic recovery theory yields an expression for B as a decreasing function of applied take-up force. Specifically, this is

$$B^6 = [B(0)]^6 - (4/\pi\lambda_{\text{eff}}/\mu D^2)F$$

where $B(0)$ is the extrudate swell in the absence of applied forces, λ_{eff} is the effective relaxation time, μ is viscosity (both evaluated at the capillary wall), and D is the spinneret capillary diameter. An experimental study of extrudate swell of several rheologically characterized melts (high-density polyethylene, low-density polyethylene, polypropylene, polystyrene) has been carried out at 180°C by four different methods (frozen, annealed in hot silicone oil, photographed emerging into air, photographed emerging through 180°C silicone oil) in the absence of applied take-up forces. Extrudate swell for a melt emerging from dies with differing diameters correlates with capillary-wall shear rate. A comparison of extrudate swell with normal stress–shear stress ratio shows the best agreement for frozen extrudates and photographs of melts emerging into air. The data is compared to the Tanner theory of extrudate swell. B has been determined during melt spinning and shown to be a function of take-up force for both a high-density polyethylene and polypropylene melt. B decreases rapidly with applied take-up stresses. The results are compared to the predictions of the partially constrained elastic recovery theory.

INTRODUCTION

When polymer melts emerge from a cylindrical die orifice, the diameter of the extrudate is generally greater than the capillary. The ratio of the extrudate diameter d to the die orifice diameter D, the swell ratio B, varies from melt to melt and is a function of extrusion rate and die length and diameter. During the melt spinning of fibers, external forces are applied to molten polymer filaments emerging from dies. It is generally found that the application of a take-up force on a polymer filament emerging from a die results in a de-

* Present address: Dow Chemical Company, Freeport, Texas.

crease in the swell ratio and a continued drawing down of the filament diameter as long as the melt temperature is high enough to maintain finite elongational flow response.[1,2] It is the purpose of this paper to present an experimental and theoretical study of extrudate swell especially of the influence of applied take-up forces on the magnitude of the swell ratio of a molten fiber emerging from a spinneret.

While as early as 1845, Brooman[3] had manufactured thread from gutta percha by taking up the descending filament with an applied tension, the history of the melt spinning process dates only to Carothers and Hill[4] in 1932. Studies of the deformation behavior during melt spinning were first made by Ziabicki and Kedzierska[1,2,5] with serious consideration of nonisothermal effects being due to Kase and Matsuo.[6] The view taken by these researchers and some more recent investigators[7-9] is that the rheological response of the melts in the spinline may be represented in terms of an elongational viscosity. However, experimental studies of the tensile stress variation in isothermal polyolefin melts during uniaxial extension find use of an elongational viscosity inadequate.[10,11,14] Nowhere on the spinline is this problem more apparent than at the exit of the spinneret where the melt swells as it emerges from the capillary. Extrudate swell has long been known in the polymer industry and suggested as due to unconstrained elastic recovery.[15-17] Analyses in terms of this mechanism have been proposed and carried through at various levels of sophistication.[16-21] In melt spinning, the recovery is not unconstrained, rather the melt recovers from Poiseuille shearing flow to a state of uniaxial stress.

This paper is based on an analysis of the spinline extrudate swell problem. Extrudates well in a spinline has received little attention and we known of no published analyses. The only study we are aware of is unpublished work of H. L. LaNieve of Celanese which has only been briefly and orally described to one of us (J.L.W.). LaNieve seems to have used a modification of the work of Nakajima and Shida.[15] We present a series of three different theoretical analyses of the problem based on (i) dimensional analysis, (ii) force–momentum balance, and (iii) partially constrained elastic recovery. We will also present experimental studies of extrudate swell in the absence and in the presence of take-up forces. This paper represents a continuation of studies at the University of Tennessee on rheological behavior and structure development during melt spinning.[11,13,22,23,24] In another recent paper,[25] we have discussed three-dimensional elastic recovery following steady flows in some detail, and parts of the present paper represent an expansion of these views.

THEORETICAL

Nonlinear Viscoelasticity

From the general theory of non-linear viscoelastic fluids[26,27] the stress tensor may be represented as a hereditary functional of the deformation history, i.e.,

$$\sigma = -p\mathbf{I} + \mathbf{F}\left[\begin{matrix} s = t \\ \text{deformation history} \\ s = -\infty \end{matrix}\right] \tag{1}$$

where the total extent of the memory may be represented through a characteristic relaxation time. Generally, eq. (1) must be expressed as a complex infinite expansion of integrals. All but the simplest flow problems prove too difficult to solve with eq. (1). Experimental studies by various research groups[11,28–30] have shown that the stress tensor in polymer solutions and melts may be represented by an equation of form

$$\sigma = -p\mathbf{I} + \int_0^\infty [m_1(z)\boldsymbol{c}^{-1} - m_2(z)\boldsymbol{c}]dz \tag{2}$$

where $m_1(z)$ and $m_2(z)$ are relaxation functions and $\boldsymbol{c}^{-1}$ and $\boldsymbol{c}$ are the Finger and Cauchy deformation tensor; $m_1(z)$ and $m_2(z)$ may be reasonably well represented by the forms

$$m_1(z) = \left(1 + \frac{\epsilon}{2}\right)\tilde{m}(z) \tag{3a}$$

$$m_2(z) = -\frac{\epsilon}{2}\tilde{m}(z) \tag{3b}$$

$$\tilde{m}(z) = \Sigma \frac{G_i}{\lambda_{i\text{eff}}} e^{-z/\lambda_{i\text{eff}}} \tag{3c}$$

where ϵ and the G_i are constants. The $\lambda_{i\text{eff}}$ are effective relaxation times which depend upon deformation or deformation rate invariants. A typical useful form of $\lambda_{i\text{eff}}$ is[26,28]

$$\lambda_{i\text{eff}} = \frac{\lambda_i}{1 + a\lambda_i \overline{\Pi_d^{1/2}(z)}} \tag{3d}$$

$$\overline{\Pi_d^{1/2}} = \frac{1}{t}\int_0^t \Pi_d^{1/2}(z)dz \tag{3e}$$

where Π_d is the second invariant of the rate of deformation tensor, a is a constant, and λ_i is the asymptote of $\lambda_{i\text{eff}}$ at low deformation rates.

In steady long duration laminar shear flow $v_1 = \Gamma x_2$, the stress components from eq. (2) give rise to three functions: a shear stress σ_{12} and two normal stress differences, N_1 and N_2:

$$\sigma_{12} = \mu\Gamma = (\Sigma G_i \lambda_{i\text{eff}})\Gamma \tag{4a}$$

$$N_1 = \sigma_{11} - \sigma_{22} = 2[\Sigma G_i \lambda_{i\text{eff}}^2]\Gamma^2. \tag{4b}$$

$$N_2 = \sigma_{22} - \sigma_{33} = \epsilon[\Sigma G_i \lambda_{i\text{eff}}^2]\Gamma^2 = \frac{\epsilon}{2}N_1. \tag{4c}$$

Dimensional Analysis

To formulate the extrudate swell problem, we must simultaneously solve the constitutive equation with a balance of forces. The differential force balance has the steady-state form[31]

$$\rho(\mathbf{v}\cdot\nabla)\mathbf{v} = \nabla\cdot\sigma. \tag{5}$$

It is useful for us to first examine the extrudate swell problem in terms of dimensional analysis. Following the traditional treatments of Newtonian fluid mechanics (see, e.g., Goldstein[32]) and studies for viscoelastic

fluids,[26,33-38] we introduce a characteristic length L and a characteristic velocity V. The dimensionless velocity field may be expressed as follows:

$$\mathbf{v} = \mathbf{v}^*\left[\frac{LV\rho}{\mu}, \frac{\lambda_{ch}V}{L}, \begin{matrix}\text{viscoelastic}\\ \text{ratio numbers,}\end{matrix} \begin{matrix}\text{dimensionless}\\ \text{position,}\end{matrix} \begin{matrix}\text{boundary}\\ \text{conditions}\end{matrix}\right] \tag{6}$$

where μ is viscosity; ρ is density; $LV\rho/\mu$ is a Reynolds number, N_{We}[32]; λ_{ch} is a characteristic time which might be taken as the maximum relaxation time of the melt; and $\lambda_{ch}V/L$ is a Weissenberg number, N_{We}.[26,33,35-38] The viscoelastic ratio numbers specify the character of the functional.

From eq. (6), it may readily be shown that the extrudate swell B, representing an integral over the free surface emerging from the spinneret, has the form

$$B = \frac{d}{D} = f\left[\frac{LV\rho}{\mu}, \lambda_{ch}\frac{V}{D}, \begin{matrix}\text{viscoelastic}\\ \text{ratio}\\ \text{numbers}\end{matrix}, \frac{L}{D}, \begin{matrix}\text{die}\\ \text{entry}\\ \text{geometry}\end{matrix}, \frac{\lambda_{ch}F}{\mu D^2}\right] \tag{7}$$

where D is the spinneret hole diameter, L is the length, d is the extrudate diameter, and F is the force applied to the emerging fluid filament. If we restrict ourselves to creeping flow which would be the case for polymer melts, the Reynolds number dependence does not appear. If we measure extrudate swell in polymer melts as a function of extrusion rate, the value of B will vary considerably from die to die depending upon the diameter, L/D, die entry geometry, etc. The functionality of B upon flow rate and these parameters will vary from fluid to fluid.

However, if we limit ourselves to a particular polymer melt and only use dies of similar geometry, i.e., L/D ratio and inlet, eq. (7) reduces to a dependence of B upon λ_{ch} V/D characteristic of the polymer and all experimental

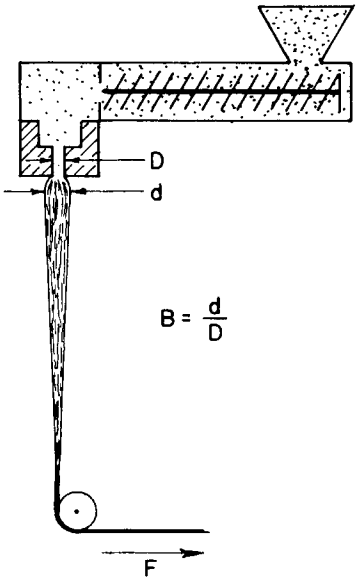

Fig. 1. Extrudate swell in the melt spinning of a fiber.

data should be normalizable by dividing the volumetric extrusion rate by the cube of the die diameter or the linear velocity by the die diameter. Equivalently, if we use Weissenberg's analysis of the capillary tube flow rate,[27,39] B would be a unique function of the capillary wall shear rate. Clearly, also, if we take the asymptote of very large L/D in which the residence time of the melt within the capillary exceeds its memory or characteristic time, then B will no longer depend upon the value of L/D or die entrance geometry, i.e.,

$$\lim_{L/D\to\infty} B = f\left(\lambda_{ch}\frac{V}{D}, \begin{matrix}\text{viscoelastic,}\\ \text{ratio}\\ \text{numbers}\end{matrix}, \frac{\lambda_{ch}F}{\mu D^2}\right). \tag{8}$$

Overall Force–Momentum Balance

Let us make an overall force–momentum and mass flux balances between the end of the capillary die where the flowing polymer fluid is in fully developed flow and a vertically descending extrudate which is being acted on gravity, air drag stresses σf, and filament tension F (see Fig. 1):

$$\int_0^R 2\pi r\rho u^2 dr - \int_0^R 2\pi r\sigma_{11} dr = \rho V_f^2 \frac{\pi d^2}{4}(x_1) + \int_0^{x_1} \pi d(x_1)\sigma_f dx_1 - \int_0^{x_1} \frac{\pi d^2}{4}(x_1)\rho g dx_1 - F \tag{9}$$

$$Q = \int_0^2 2\pi r u dr = \frac{\pi D^2}{4} v = \frac{\pi d^2}{4}(x_1) V_f(x_1). \tag{10}$$

Equation (9) contains a number of interesting special cases. If we equate the right hand of eq. (9) at position x_1 and position L at take-up device, the spinline force balance of Ziabicki and Kedzierska[1,2,5] is obtained. In terms of $F(x_1)$, this is

$$F(x_1) = F(L) - \int_{x_1}^{L} \frac{\pi d^2}{4}(x_1)\rho g dx_1 - \int_{x_1}^{L} \pi d(x_1)\sigma_f dx_1 + \frac{\pi d^2}{4}(x_1)\rho V_f^2(x_1) - \frac{\pi d^2}{4}(L)\rho V_f^2(L). \tag{11}$$

For significant momentum flux but zero normal stress σ_{11} gravity, air drag, and take-up force F, Harmon's[40,41] theory of jet expansion may be obtained from Eq. (9):

$$\left(\frac{D^2}{d}\right) = \frac{1}{B^2} = \int_0^1 2\frac{r}{R}\left(\frac{u}{v}\right)^2 d\frac{r}{R}. \tag{12}$$

where v is the average velocity within the capillary.

If we allow now for both normal stress[42,43] and take-up force;

$$\left(\frac{D}{d}\right)^2 = \frac{1}{B^2} = \int_0^R 2\frac{r}{R}\left(\frac{u}{v}\right)^2 d\frac{r}{R} - \frac{1}{\rho v^2}\left[\bar{\sigma}_{11} - \frac{F}{\pi D^2/4}\right] \tag{13a}$$

with

$$\bar{\sigma}_{11} = \int_0^1 2\frac{r}{R}\sigma_{11}(r) dr \tag{13b}$$

For the case of F equal to zero, we obtain the theory of Metzner et al.[43] We may write eq. (13a) in the equivalent forms:

$$\frac{1}{B^2} = \left[\frac{1}{B(0)}\right]^2 + \frac{4}{\pi}\frac{F}{D^2v^2\rho} \tag{14a}$$

$$= \left[\frac{1}{B(0)}\right]^2 + \frac{4}{\pi}\left(\frac{1}{N_{\mathrm{Re}}N_{\mathrm{We}}}\right)\frac{\lambda_{\mathrm{ch}}F}{\mu D^2}. \tag{14b}$$

From eqs. (13) and (14) we see that the influence of applied take-up force $F(L)$ is to decrease B. It is also of interest to see that the extent of decrease of swell does not depend upon rheological properties but only applied take-up stress and momentum flux. In eq. (14b), we note that this dependence can be expressed in terms of the dimensionless groups of eq. (7) including the Reynolds and Weissenberg numbers and $\lambda_{ch}F/\mu D^2$.

Zero Momentum Flux Asymptote

The above comments are based on $\bar{\sigma}_{11}$ being independent of F. We therefore need to further investigate the normal stress $\bar{\sigma}_{11}$ within the capillary. Following Lodge,[42] we divide the normal stress in eq. (13b) into pressure p and extra stress σ_{11} terms and eliminate the pressure with the radial component of the equation of motion:

$$0 = -\frac{\partial p}{\partial r} + \frac{\partial \tau_{22}}{\partial r} + \frac{\tau_{22} - \tau_{33}}{r}. \tag{15}$$

If we now integrate by parts, it may be shown that

$$\bar{\sigma}_{11} = \sigma_{22}(R) + \int_0^1 \frac{r}{R}(2N_1 + N_2)d\frac{r}{R} \tag{16}$$

where $\sigma_{22}(R)$ is the radial normal stress at the outer radius of the capillary (i.e., the negative of a transducer measured pressure). We may now see that our comments that increasing F decreases B is based on changes in $\sigma_{22}(R,L)$ being small.

For negligible momentum flux, we obtain from eq. (9)

$$\bar{\sigma}_{11} = \frac{F}{\pi D^2/4}. \tag{17}$$

It seems clear from eqs. (16) and (17) that all we obtain from the force balance is that increasing F should increase σ_{22}(R,L) or decrease ($-\sigma_{22}(R,L)$) the pressure measured at the end of the die. Measurements of this exit pressure in polymer melts have been made by Han and Charles[44] who find it to be significantly large and positive. The influence of take-up forces would be to decrease the exit pressure and push it toward atmospheric.

Elastic Recovery Theory of Extrudate Swell Under Tension

In this section, we will develop an approximate theory of extrudate swell of molten polymers emerging from dies. We neglect momentum fluxes and

consider extrudate swell as partially unconstrained elastic recovery. Our calculations of recovery will use the methods of Lodge[42] (compare White[25]), and they will be fitted into a theory of extrudate swell in the manner developed by Tanner.[21] Our arguments are as follows.

Consider a viscoelastic fluid defined by eqs. (2) and (3) to be at rest until time 0, at which time it is subjected to a deformation which continues until time t_R when the stress is released to a new state $\sigma(t)$ and the material exhibits an unconstrained three-dimensional partial recovery. At some time $t > t_R$, we may write

$$\sigma(t) = p\mathbf{I} + \underbrace{\int_0^{t-(t_R+\delta t_R)} [m_1(z)\boldsymbol{c}^{-1} - m_2(z)\boldsymbol{c}]dz}_{\text{period of delayed recovery}} + \underbrace{\int_{t-(t_R+\delta t_R)}^{t-t_R} [m_1(z)\boldsymbol{c}^{-1} - m_2(z)\boldsymbol{c}]dz}_{\text{period of instantaneous recovery}} + \underbrace{\int_{t-t_R}^{t} [m_1(z)\boldsymbol{c}^{-1} - m_2(z)\boldsymbol{c}]dz}_{\text{period of steady flow}} + \underbrace{\int_t^{\infty} m_1(z)dz(\boldsymbol{c}^{-1})^+ - \int_t^{\infty} m_2(z)dz(\boldsymbol{c})^+}_{\text{period prior to deformation}} \quad (18)$$

where the integral form $t - (t_R + \delta t_R)$ to $t - t_R$ represents the period of instantaneous elastic recovery following the release of the applied stresses. This will be of infinitesimal order and may be neglected. The quantities $(\boldsymbol{c}^{-1})^+$ and $(\boldsymbol{c})^+$ represent the total deformation from time 0 to time t.

In order to proceed, several simplications need to be made. These are: (i) ϵ is zero and $m_2(z)$ may be neglected; (ii) $m_1(z)$ may be represented as a single exponential; (iii) the deformation in the capillary is of long duration and entrance effects in the die may be neglected. Assumption (iii) allows us to neglect the fourth term of eq. (18) and as shown by Lodge,[42] assumption (ii) allows us to neglect the first term. This leaves us with only the third term with the upper limit going to infinity.

Equation (18) is difficult to work with, for we must define the deformation precess in terms of an unknown reference state existing after the recovery. If, however, we change the reference state from the state following the recovery to the one just before the stress we released, calculations are much simplified. This leads to

$$\boldsymbol{Q}(\sigma + p\mathbf{I})\boldsymbol{Q}^T = \int_0^{\infty} m_1(z)\boldsymbol{Q}\boldsymbol{c}^{-1}\boldsymbol{Q}^T dz \quad (19)$$

where $\boldsymbol{Q}$ and $\boldsymbol{Q}^T$ are appropriate transformation matrices. From $\boldsymbol{Q}$ and Q^T we may define a recoverable deformation tensor applicable to *unconstrained* recoveries, i.e.,[21,25]

$$(\boldsymbol{c}^{-1})^* = \boldsymbol{Q}\boldsymbol{Q}^T \quad (20)$$

Of special interest is the three-dimensional recovery from simple shear flow

and Poiseuille flow because of its application to extrudate swell. For simple shear flow, the kinematics may be specified by

$$\frac{dx}{dt} = \Gamma x_2 \qquad \frac{dx_2}{dt} = \frac{dx_3}{dt} = 0 \tag{21}$$

$$\boldsymbol{Q}\boldsymbol{c}^{-1}\boldsymbol{Q}^T = \begin{vmatrix} 1 + \Gamma^2 z^2 & \Gamma z & 0 \\ \Gamma z & 1 & 0 \\ 0 & 0 & 1 \end{vmatrix}. \tag{22}$$

Substitution into eq. (19) restricting ourselves to long duration flows and integrating yields

$$\boldsymbol{Q}(\boldsymbol{\sigma} + p\mathbf{I})\boldsymbol{Q}^T = G\begin{vmatrix} 1 + 2\lambda_{\text{eff}}{}^2\Gamma^2 & \lambda_{\text{eff}}\Gamma & 0 \\ \lambda_{\text{eff}}\Gamma & 1 & 0 \\ 0 & 0 & 1 \end{vmatrix}. \tag{23}$$

The above analysis is for simple shear flow, but we can with no great difficulty transform it to cylindrical coordinates to handle the problem of recovery from fully developed Poiseuille flow. Now taking x_1 as the axial direction, r as the radial direction, and θ as the angular direction (compare Tanner[21]), the most general deformation of an untwisted cylinder is

$$\begin{aligned} x_1(t) &= \alpha_1 x_1(t_R) - g(r) \\ r(t) &= \alpha_2 r(t_R) \qquad\qquad \alpha_2 = \frac{1}{\sqrt{\alpha_1}} \\ \theta(t) &= \theta(t_R) \end{aligned} \tag{24}$$

where $g(r)$ represents an $x_1 - r$ shearing deformation. Using eq. (24) to evaluate $\boldsymbol{Q}$ and presuming the various annuli of fluid are held in tension with stress $\sigma_t(r)$, we may rewrite the left-hand side of Eq. (23) as follows

$$\boldsymbol{Q}(\boldsymbol{\sigma} + p\mathbf{I})\boldsymbol{Q}^T = p\begin{vmatrix} \frac{1}{\alpha_1{}^2}\frac{\sigma_t}{p} + 1 + g'^2 & \frac{1}{\alpha_2}g' & 0 \\ \frac{1}{\alpha_2}g' & \frac{1}{\alpha_2{}^2} & 0 \\ 0 & 0 & \frac{1}{\alpha_2{}^2} \end{vmatrix} \tag{25}$$

where g' is dg/dr. Equating eqs. (23) and (25) leads to

$$\begin{aligned} \frac{1}{\alpha_1{}^2}\sigma_t + p + pg'^2 &= G[1 + 2\lambda_{\text{eff}}{}^2\Gamma^2] \\ p\frac{1}{\alpha_2}g' &= G\lambda_{\text{eff}}\Gamma \\ p\frac{1}{\alpha_2{}^2} &= G. \end{aligned} \tag{26}$$

From eqs. (26), we obtain

$$\alpha_2^4(\sigma_t + G\alpha_2^2) + G\lambda_{\text{eff}}\Gamma^2 = G[1 + 2\lambda_{\text{eff}}^2\Gamma^2]$$

or

$$\alpha_2^6 + \frac{\sigma_t}{G}\alpha_2^4 = [1 + \lambda_{\text{eff}}^2\Gamma^2]. \tag{27}$$

Integration of eq. (27) across the cross section and presuming that α_2 is independent of radius leads to

$$\frac{\pi d^2}{4}B^6 + \frac{F}{G} + B^4 = \int_0^{d/2} 2\pi r(1 + \lambda_{\text{eff}}^2\Gamma^2)dr \tag{28}$$

where we have interpreted the integral of σ_t across the extrudate as being the applied force. Noting [compare eq. (23)] that the shear stress in steady shear flow in a tube is for this model $G\lambda_{\text{eff}}\Gamma$ and that from the axial component of the equation of motion for fully developed Poiseuille flow in a tube[27]

$$\frac{\sigma_{12}(r)}{\sigma_{12}(R)} = \frac{r}{R} \text{ and } \lambda_{\text{eff}}^2\Gamma^2 = \frac{\sigma_{12}^2}{G^2} = \left[\frac{\sigma_{12}(R)}{GR}\right]^2 r^2 \tag{29}$$

we may integrate eq. (28) to give

$$B^6 + \frac{\bar{\sigma}_t}{G}B^4 = 1 + \frac{1}{2}\left[\frac{\sigma_{12}(R)}{G}\right]^2 = 1 + \frac{1}{2}[\lambda_{\text{eff}}\Gamma]^2(R) \tag{30}$$

where $\bar{\sigma}_t$, the average tensile stress in the extrudate, is the ratio of F to $\pi d^2/4$.

Let us now interpret these results. First the case where the force F is equal to zero

$$B(0) = \left[1 + \frac{1}{2}\left[\frac{\sigma_{12}(R)}{G}\right]^2\right]^{1/6} = \left[1 + \frac{1}{2}[\lambda_{\text{eff}}^2\Gamma(R)]^2\right]^{1/6}$$
$$= \left[1 + \frac{1}{2}\left[\frac{(N_1)_w}{2(\sigma_{12})_w}\right]^2\right]^{1/6} \tag{31}$$

where we have used eq. (4). This is equivalent to Tanner's earlier result.[21] When the force F is not equal to zero,

$$B^6 + \frac{\bar{\sigma}_t}{G}B^4 = [B(0)]^6 \tag{32a}$$

or

$$B^6 = [B(0)]^6 - \frac{4}{\pi}\frac{\lambda_{\text{eff}}F}{\mu D^2} \tag{32b}$$

In eq. (32b), μ and λ_{eff} refer to the fluid at the capillary wall before it emerges. Note the occurrence of the dimensionless group $\lambda_{\text{eff}}F/\mu D^2$ which occurs in eqs. (7), (8), and (14b).

Again we see that the influence of take-up forces on extrudate swell is to decrease the swell. Equations (13) and (14) and (32) agree as to the influence of applied forces but differ to the exact analytical form.

We suspect but have not proven that eq. (32) or at least the general character of its detailed derivation remains valid where short L/D dies are used and die entry flow influences B.

We now turn to experimental studies of extrudate swell.

RHEOLOGICAL CHARACTERISTICS OF POLYMER MELTS STUDIED

Materials

Five commercial polymers were used in this study. These were a polystyrene (PS) (Dow Styron 678), an isotactic polypropylene (PP) (Hercules Profax 6523), a low-density polyethylene (LDPE) (Dow 310 M, MI = 5.0), and two high-density polyethylenes (5.0-HDPE, Phillips Marlex EMB 6050; and 0.1-HDPE, Phillips Marlex EHM 6001).

Rheological Characterization

The non-Newtonian shear viscosity μ and the first normal stress difference N_1 of the five polymer melts were determined at 180°C in the low shear rate region with the Weissenberg rheogoniometer. If 1 is the direction of flow; 2, the direction of shear; and Γ, the shear rate, then[27,42]

$$\Gamma = \frac{\Omega}{\tan\psi} \tag{33a}$$

$$\sigma_{12} = \mu\Gamma = \frac{3M}{2\pi R^3} \tag{33b}$$

$$N_1 = \frac{2F}{\pi R^2} \tag{33c}$$

where Ω is the rotor rotation rate, ψ is the cone angle, R is the rotor radius, M is the torque, and F is the force pushing apart the platens. A 3°56′ cone of 2.5 cm diameter was used in the measurements. The shear rates were generally restricted to values of 1 sec^{-1} and below because of disturbances in the gap between the cone and plate.[45–47]

The non-Newtonian viscosity function μ was measured in a higher shear rate region at 180°C using an Instron capillary rheometer installed in a floor model Instron University Testing Apparatus. This is the same apparatus used in our earlier studies.[46,47] The capillary-wall shear stress was determined from a plot of the total pressure p_T required to force through a die of length–diameter ratio L/D through the expression[46–48]

$$p_T = 4(\sigma_{12})_w \frac{L}{D} + \Delta p_e \tag{34}$$

where Δp_e is the pressure loss at the die entry and the subscript w represents evaluation at the capillary wall. The shear rate at the capillary wall was determined through Weissenberg's relationship[27,39]

$$\Gamma_w = \left(-\frac{du}{dr}\right)_w = \left(\frac{3n' + 1}{4n'}\right)\frac{320}{\pi D^3} = \left(\frac{3n' + 1}{4n'}\right)\frac{8V}{D} \tag{35}$$

where

$$n' = \frac{d \log(\sigma_{12})_w}{d \log 32Q/\pi D^3}$$

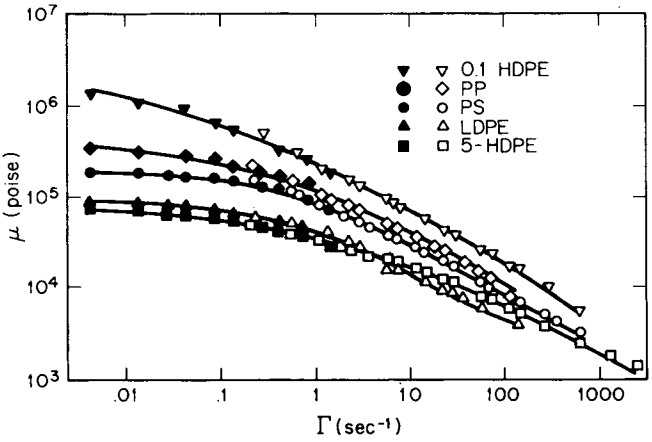

Fig. 2. Non-Newtonian viscosity μ as a function of shear rate Γ (180°C). Solid points are rheogoniometer data. Open points are capillary data.

where Q is the volumetric extrusion rate and u is the local axial velocity within the capillary.

Results

The non-Newtonian viscosity function of the five melts studied are contained in Figure 2. The results are similar to data for these types of polymer melts contained in the literature.[16,24,26,27,46,47] The melts were found to be

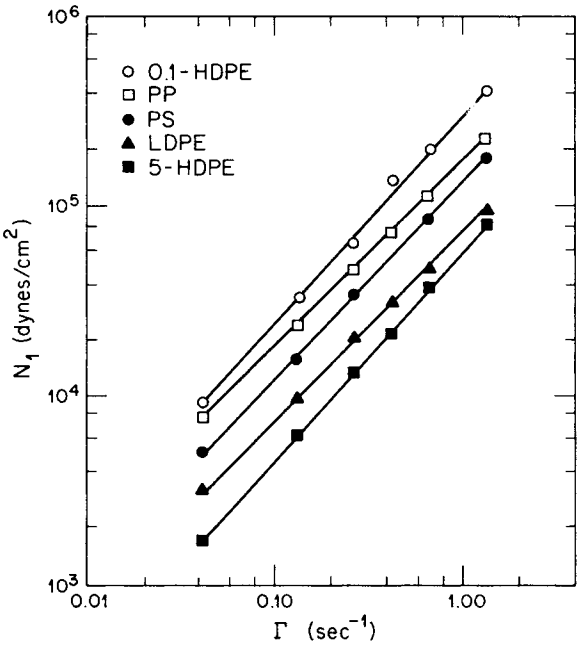

Fig. 3. Principal normal stress difference N_1 as a function of shear rate Γ (180°C).

Newtonian at low shear rates, and the viscosities decrease with increasing shear rate. The viscosities order according to

$$0.1\text{-HDPE} > \text{PP} > \text{PS} > \text{LDPE} \sim 5\text{-HDPE}.$$

The viscosities of the LDPE and 5-HDPE are similar. At low shear rates, the LDPE is a more viscous, but there is a crossover at intermediate shear rates.

The principal normal stress data N_1 for the five melts is summarized in Figure 3 as a function of shear rate. The results are again qualitatively similar to those of other researchers[45–47] with the normal stresses increasing more rapidly than the shear stress. The data order according to

$$0.1\text{-HDPE} > \text{PP} > \text{PS} > \text{LDPE} > 5\text{-HDPE}.$$

EXPERIMENTAL STUDY OF EXTRUDATE SWELL IN THE ABSENCE OF APPLIED STRESSES

These experiments were carried out at 180°C using our Instron capillary rheometer. Measurements were carried out using a series of eight capillaries with diameters ranging from 0.023 to 0.080 in. and L/D ratios ranging from 5.0 to 47.5.

The extrudate swell of the unstressed extrudate from the Instron capillary rheometer were measured by *four* different techniques. First, the frozen extrudate diameter was measured using a micrometer. Secondly, the solidified extrudates were annealed in hot silicone oil at temperatures above the melting or glass transition temperature. For the polyethylenes and PS, the temperature used was 160°C, while for the PP which melts at about 165°C, the temperature used was 180°C. The samples were annealed for approximately 15 min after which period they had achieved a constant diameter. The extrudates were removed and measured with a micrometer.

A third technique used was direct photographs of the extrudate as it emerged from the capillary. A 35-mm camera with fine-grain film was used. The negatives were blown up on a grid screen using a slide projector and the diameters measured. Here, one must be wary as gravity will tend to decrease to extrudate swell below its true value.

The fourth method of measurement was to extrude the melt into a bath of silicone oil at 180°C in an effort to approximate isothermal behavior. Photographs of the extrudate in the bath were taken between 5 and 10 min after the extrudate emerged from the capillary.

Results

The first point which required a decision was the proper manner of plotting extrudate swell data for the various melts under study. For zero applied tension and negligible Reynolds numbers, eq. (7) suggests that $B(0)$ for any specific melt should correlate with V/D when dies of varying diameter but equal L/D ratio are studied. From eq. (37), this is equivalent to representing $B(0)$ as a function of capillary wall shear rate Γ_w. We studied the "frozen" extrudate swell of the melts, particularly the 5-HDPE melt, as a function of

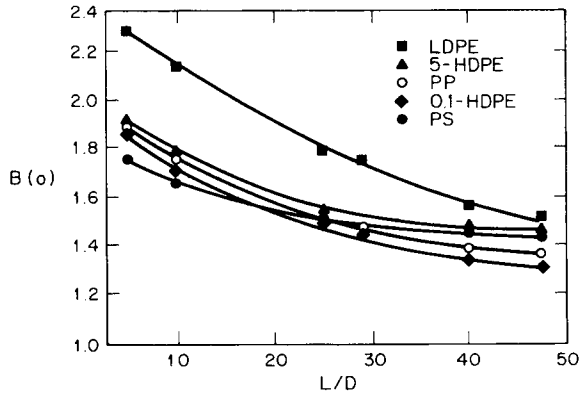

Fig. 4. Frozen extrudate swell $B(0)$ for five polymer melts as a function of L/D ratio at constant shear rate at 180°C.

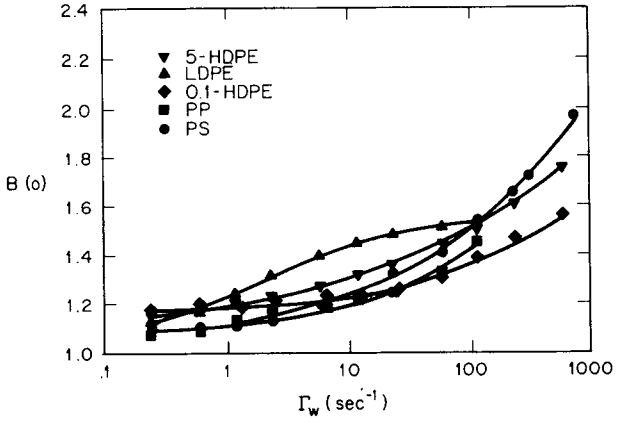

Fig. 5. Frozen extrudate swell $B(0)$ for five polymer melts as a function of capillary wall shear rate $\dot{\Gamma}_w$.

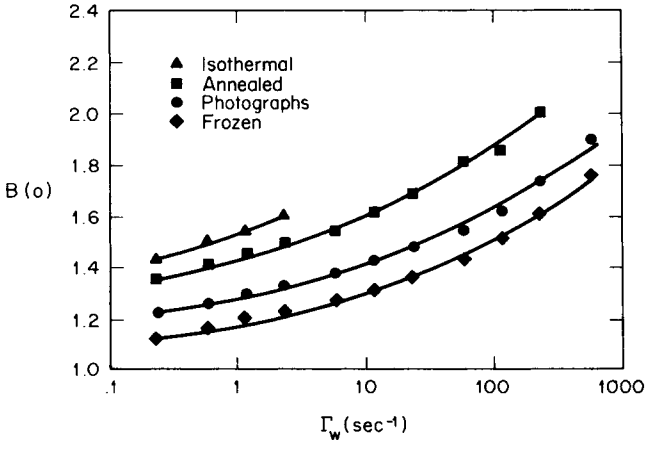

Fig. 6. Variation of extrudate swell $B(0)$ for the 5-HDPE depending upon the method of measurement: (1) frozen extrudates; (2) extrudates annealed at 160°C in hot silicone oil; (3) photographs extrudates emerging from capillary; (4) photographs of extrudates in hot silicone oil.

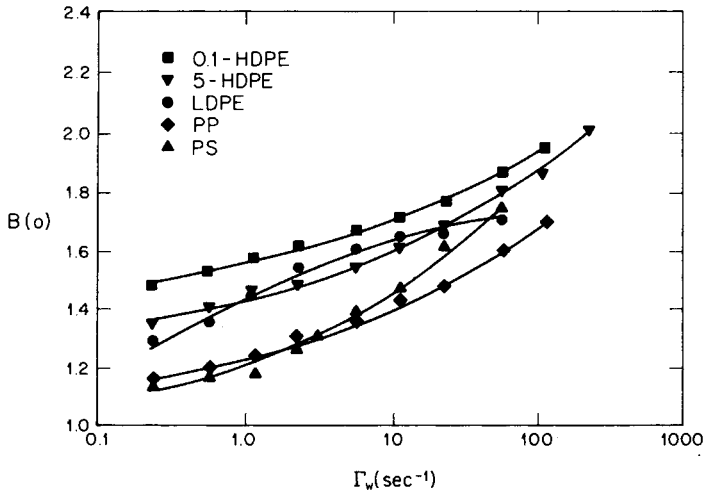

Fig. 7. Stress relieved extrudate swell data of five polymer melts as a function of shear rate.

extrusion rate, extrusion velocity, and capillary wall shear rate Γ_w. Only Γ_w was found to correlate data obtained from different diameter dies.

The variation of frozen extrudate swell with L/D ratio for the five polymer melts at a fixed Γ_w is shown in Figure 4. $B(0)$ decreases with increasing L/D, with the rate of decrease being greater for the LDPE compared to the other melts. The value of $B(0)$ for the LDPE is larger, especially for the smaller L/D dies. In Figure 5, we plot the frozen extrudate $B(0)$ for the largest L/D dies as a function of Γ_w for the five melts.

The variation of magnitude of extrudate swell with the type of measurement is shown in Figure 6 for the 5-HDPE. The values are largest for the isothermal extrusion into hot silicone oil and lowest for the frozen extrudates. The frozen extrudates and the photographed melt emerging into air from the

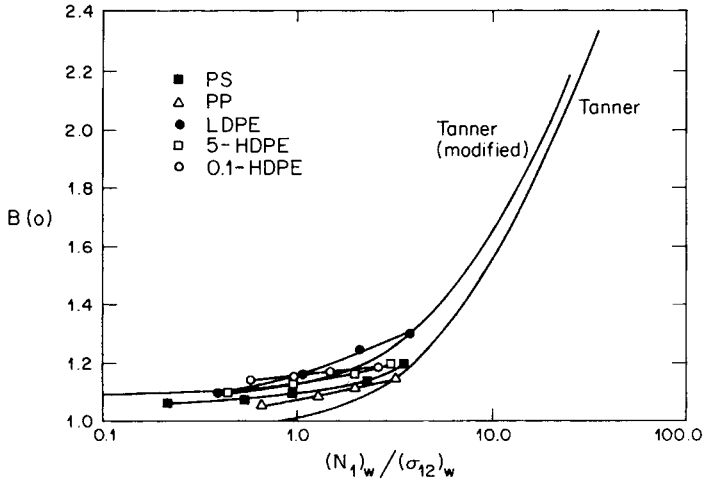

Fig. 8. Frozen extrudate swell for five melts as a function of $(N_1)/\sigma_{12})_w$ determined at capillary wall shear rate together with eqs. (31) and (36).

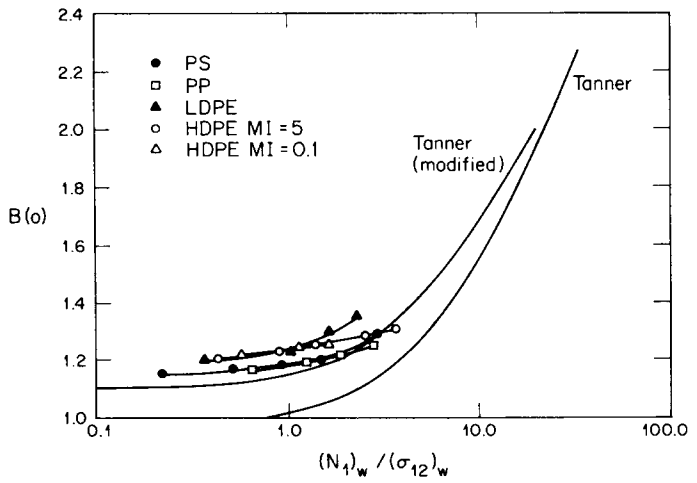

Fig. 9. Photographed emerging extrudate swell $B(0)$ for five melts as a function of $(N_1)_w/(\sigma_{12})_w$ determined at capillary-wall shear rate together with eqs. (31) and (36).

Instron rheometer represent extrudates with frozen in residual stresses. The frozen extrudates annealed in hot silicone oil and the melts extruded directly into the same fluid represent stress relieved samples. As the data from two of the samples are measured at room temperature and two at 180°C, it should be suspected that the four sets of data may be represented by two curves. As noted, for example, by Mendelson, Finger, and Bagley,[20] there is a density ratio of $\rho(20°C)/\rho(180°C)$ of 1.26 for HDPE and 1.21 for LDPE. To normalize all extrudate swell at 180°C the 20°C data should be multiplied by a factor $[\rho(20°C)/\rho(180°C)]^{1/3}$. Corrections of this magnitude are able to successfully bring together the four sets of data into two curves. In Figure 7, we contrast the stress-relieved $B(0)$ data (at 20°C) as a function of capillary-wall

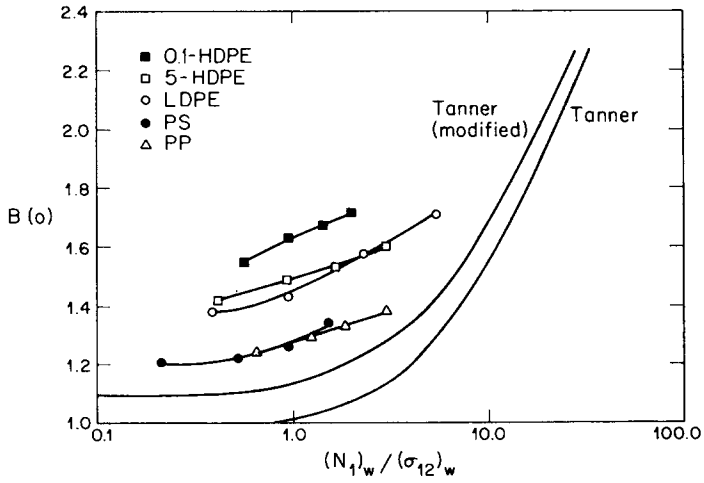

Fig. 10. Photographed emerging extrudates swell into an isothermal silicone both at 180°C as a function of $(N_1)_w/(\sigma_{12})_w$. Five melts are included in the study together with eqs. (31) and (36).

shear rate. It may be seen that the data are more widely separated than the frozen extrudate results. The polyethylenes exhibit much greater recovery in the annealing process than the polypropylene or polystyrene.

Intuitively, extrudate swell may be interpreted in terms of elastic recovery, and this is the basis for the analyses of the earlier parts of this paper. We now inquire as to how well we are able to interpret our experimental data in this light. From eq. (31), we see that according to the formulation of the extrudate swell problem (in the absence of take-up forces) which was discussed earlier, $B(0)$ should be a unique function of $\lambda_{\text{eff}}\Gamma$ or $(N_1)_w/(\sigma_{12})_w$, L/D plus various viscoelastic ratio numbers. In Figure 8, we plot $B(0)$ versus the normal stress–shear stress ratio for the solid frozen extrudates from the largest L/D dies. In Figure 9, we plot $B(0)$ obtained from photographs of extrudates emerging into air versus $(N_1)_w/(\sigma_{12})_w$, while in Figure 10, we plot $B(0)$ obtained for the melts emerging into hot silicone oil. Again, the $B(0)$ data are for the longest L/D dies. A closer correlation is found for the photographed extrudates than for those equilibrated in silicone oil. This is superficially in disagreement with the results of Mendelson et al.,[20] but it must be remembered that these authors only consider various high-density polyethylenes and the materials included in their study actually are more similar to each other than the 5-HDPE and 0.1-HDPE of our study.

We have also contrasted the data of this paper with the theory of extrudate swell that we have discussed. In Figures 8–10, we have plotted eq. (31), the result of Tanner's extrudate swell theory together with the modification

$$B(0) = C + \left[1 + \frac{1}{2}\left[\frac{(N_1)_w}{2(\sigma_{12})_w}\right]^2\right]^{1/6} \tag{36}$$

recommended by this author.[21] The additional C arises from the swell found in creeping flow of a Newtonian fluid. This was taken to be 0.1. The agreement may be seen to be best for eq. (36) with the frozen extrudates. The predictions seem a bit low for the photographed extrudates, but the agreement could be improved by increasing the additive constant C. For the melts extruded into hot silicone oil, an increase of C can account for the polypropylene and polystyrene data but not the polyethylenes. In Tanner's original paper, he made comparisons primarily with polystyrene melts. Vlachopoulos, Horie, and Lidorikis[49] also made study of extrudate swell which showed reasonably good agreement for eqs. (31). However, here again polystyrene was used.

EXPERIMENTAL STUDY OF EXTRUDATES SWELL IN THE PRESENCE OF TAKE-UP FORCE

Experimental

This study was limited to three polymers: PP, 5-HDPE, and 0.1-HDPE. These are the same polymers investigated in various University of Tennessee studies of melt spinning.[24,50] The melts were delivered from a 1-in. Modern Plastics Machinery screw extruder used in our earlier studies[11,13,22] through screens, a Zenith metering pump, and into a capillary die with a diameter 0.062 in. and L/D ratio of 10. The fiber was wound up on a spool, and ten-

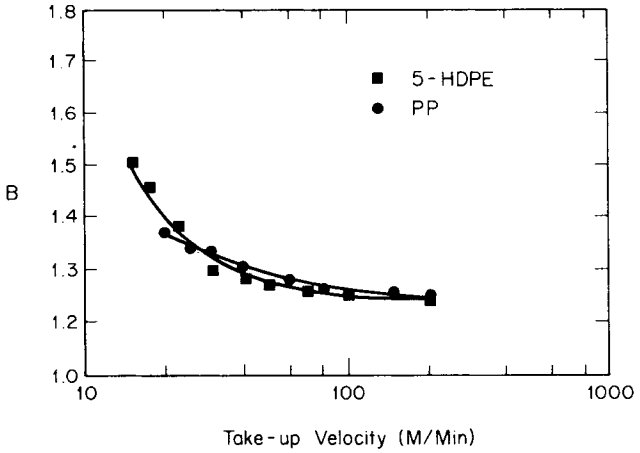

Fig. 11. Photographed extrudate swell as a function of take-up velocity for two polymer melts at 180°C.

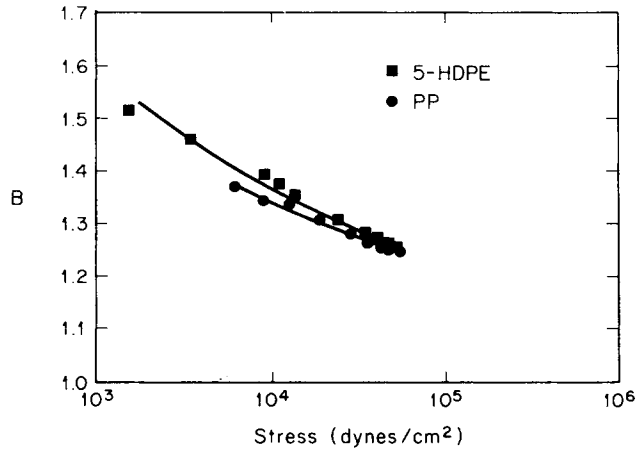

Fig. 12. Photographed extrudate swell as a function of take-up stress $F/(\pi d^2/4)$ for two polymer melts.

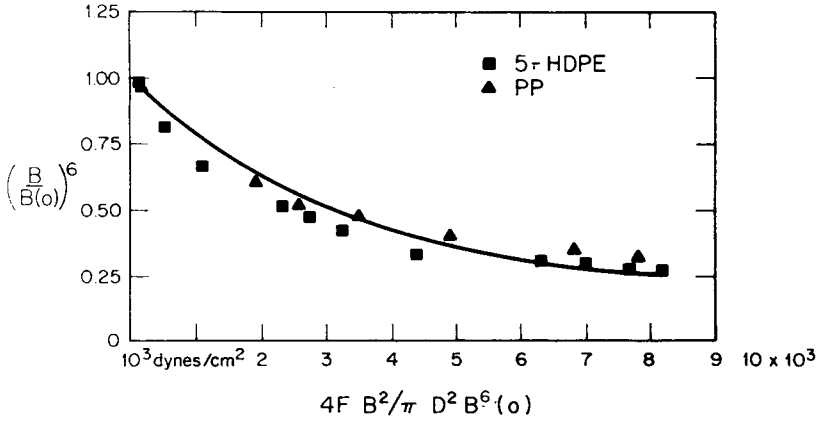

Fig. 13. Comparison of influence of take-up force on extrudate swell with eq. (37).

sions in the lower part of the spinline were measured with a Rothschild tensionmeter.[11,13,23] Photographs were taken of the melt as it emerged from the capillary. The diameter was measured at the point of maximum swell about 0.2 in. below the capillary.

Results

Of the three melts studied, only two, the 5-HDPE and the PP, were spinnable. The 0.1-HDPE broke at very low take-up velocities and indeed apparently at very low spinline tensions. The variations of extrudate swell with both take-up velocity and tensile stress (determined at the cross section of maximum swell) are plotted in Figures 11 and 12. The results for the two melts are very similar. These indicate a rapid decrease in extrudate swell with increasing take-up velocity and take-up force which is in agreement with Ziabicki and Kedzierska[1,2] and other earlier researchers.

Interpretation

In eq. (32), we derived an expression for the variation of B with applied take-up force. This may be rewritten as follows:

$$\left[\frac{B}{B(0)}\right]^6 = 1 - \frac{\lambda_{\text{eff}}}{\mu}\frac{4F}{\pi D^2}\frac{B^2}{B^6(0)}. \tag{37}$$

In Figure 13, we have plotted $[B/B(0)]^6$ as a function of $4FB^2/\pi D^2 B^6(0)$. The data for the two melts correlate well, but the plot is not linear. However, this should not necessarily be expected because the coefficient in eq. (37) contains rheological properties and the theory is approximate. From Figure 13, we predict values of λ_{eff} for the HDPE and PP in the range of 0.8 to 6.0 sec if we use capillary-wall shear rate data. From N_1 and μ data, we predict values from 0.4 to 3.3 sec. All in all, these comparisons are very encouraging.

One must be a bit wary of the above interpretation because (1) the approximate nature of the theory and (2) the L/D ratio of the die in this study is only 10, which is too small to expect a formulation of this problem which excludes the die entry flow to be a completely proper representation.

The authors would like to thank R. L. Ballman and R. A. Mendelson for helpful comments and criticism of parts of this work, and the Dow Chemical Company, Phillips Petroleum Company, and Hercules for supplying the polymers used in this study.

This research was supported in part by the National Science Foundation under Research Grant GK 18897.

References

1. A. Ziabicki and K. Kedzierska, *Kolloid-Z.*, **171**, 111 (1960).
2. A. Ziabicki, in *Man-Made Fibers*, ed. by H. Mark, S. Atlas, and E. Carnie, Wiley, New York, 1967.
3. R. A. Brooman, Brit. Pat. 10,582 (1845).
4. W. H. Carothers and J. W. Hill, *J. Amer. Chem. Soc.*, **54**, 1579 (1932).
5. A. Ziabicki and K. Kedzierska, *Kolloid-Z.*, **171**, 51 (1960).

6. S. Kase and T. Matsuo, *J. Poly. Sci.*, **3,** 2541 (1965).
7. I. Hamana, M. Matsui, and S. Kato, *Melliand* Textilber., **5,** 499 (1969).
8. T. Ishibashii, K. Aoki, and T. Ishii, *J. Appl. Polym. Sci.*, **14,** 1597 (1970).
9. C. D. Han and R. R. Lamonte, *Trans. Soc. Rheol.*, **16,** 447 (1972); *J. Appl. Polym. Sci.*, **16,** 3285 (1972).
10. H. Chang and A. S. Lodge, *Rheol. Acta*, **11,** 127 (1972).
11. I. J. Chen, G. E. Hagler, L. E. Abbott, D. C. Bogue, and J. L. White, *Trans. Soc. Rheol.*, **16,** 473 (1972).
12. T. Takaki and D. C. Bogue, *J. Appl. Polym. Sci.*, **19,** 419 (1975).
13. D. Acierno, J. N. Dalton, J. M. Rodriguez, and J. L. White, *J. Appl. Polym. Sci.*, **15,** 2395 (1971).
14. J. A. Spearot and A. B. Metzner, *Trans. Soc. Rheol.*, **16,** 495 (1972).
15. J. H. Dillon and N. Johnston, *Physics*, **4,** 225 (1933).
16. R. S. Spencer and R. E. Dillon, *J. Colloid Sci.*, **3,** 163 (1948).
17. N. Nakajima and M. Shida, *Trans. Soc. Rheol.*, **10,** 299 (1966).
18. D. L. McIntosh, Ph.D. Dissertation, Washington University, St. Louis, Missouri, 1960.
19. W. W. Graessley, S. D. Glasscock, and R. L. Crawley, *Trans. Soc. Rheol.*, **14,** 519 (1970).
20. R. A. Mendelson, F. L. Finger, and E. B. Bagley, *J. Polym. Sci.*, **C35,** 177 (1971).
21. R. I. Tanner, *J. Polym. Sci. A-2*, **9,** 2067 (1970).
22. L. E. Abbott and J. L. White, in *U.S. Japan Seminar on Polymer Processing and Rheology*, ed. by D. C. Bogue, M. Yamamoto, and J. L. White, *Appl. Polym. Symp.*, **20,** 247 (1973).
23. J. R. Dees and J. E. Spruiell, *J. Appl. Polym. Sci.*, **18,** 1053 (1974).
24. J. L. White, K. C. Dharod, and E. S. Clark, *J. Appl. Polym. Sci.*, **18,** 2539 (1974).
25. J. L. White, *Trans. Soc. Rheol.*, **19,** 271 (1975).
26. D. C. Bogue and J. L. White, Engineering Analysis of Non-Newtonian Fluids, NATO Agardograph 144, 1970.
27. S. Middleman, *The Flow of High Polymers*, Wiley, New York, 1968.
28. I. J. Chen and D. C. Bogue, *Trans. Soc. Rheolo.*, **16,** 58 (1972).
29. P. J. Carreau, *Trans. Soc. Rheol.*, **16,** 99 (1972).
30. E. B. Christiansen and W. R. Leppard, *Trans. Soc. Rheol.*, **18,** 65 (1974).
31. C. Truesdell and R. A. Toupin, in *Handbuch der Physik*, Vol. III/1, Springer Verlag, Berlin, 1960.
32. S. Goldstein, *Modern Developments in Fluid Dynamics*, Clarendon Press, Oxford, 1938.
33. J. L. White, *J. Appl. Polym. Sci.*, **8,** 2339 (1964).
34. C. Truesdell, *Phys. Fluids*, **7,** 1134 (1964).
35. A. B. Metzner, J. L. White, and M. M. Denn, *A.I.Ch.E. J.*, **12,** 863 (1966).
36. D. C. Bogue and J. Doughty, *Ind. Eng. Chem., Fundam.*, **5,** 243 (1966).
37. J. L. White and N. Tokita, *J. Appl. Polym. Sci.*, **11,** 231 (1967).
38. J. L. White, *Rubber Chem. Technol.*, **42,** 257 (1969).
39. R. Eisenschitz, B. Rabinowitsch, and K. Weissenberg, *Mitt deut Materialpruf*, **9,** 91 (1929).
40. D. B. Harmon, *J. Franklin Inst.*, **259,** 519 (1955).
41. S. Middleman and J. Gavis, *Phys. Fluids*, **4,** 355 (1961).
42. A. S. Lodge, *Elastic Liquids*, Academic Press, New York, 1964.
43. A. B. Metzner, W. T. Houghton, R. A. Sailor, and J. L. White, *Trans. Soc. Rheol.*, **5,** 133 (1961).
44. C. D. Han and M. E. Charles, *Trans. Soc. Rheol.*, **14,** 700 (1970); *ibid.*, **15,** 371 (1971).
45. R. A. King, *Rheol. Acta*, **5,** 35 (1966).
46. T. F. Ballenger, I. J. Chen, G. E. Hagler, D. C. Bogue, and J. L. White, *Trans. Soc. Rheol.*, **15,** 195 (1971).
47. B.-L. Lee and J. L. White, *Trans. Soc. Rheol.*, **18,** 467 (1974).
48. E. B. Bagley, *J. Appl. Phys.*, **28,** 624 (1957).
49. J. Vlachopoulos, M. Horie, and S. Lidorikis, *Trans. Soc. Rheol.*, **16,** 669 (1972).
50. H. Henson and J. E. Spruiell, unpublished research.

Received January 31, 1975
Revised July 21, 1975